Journal of Cleaner Production 208 (2019) 373–383

Contents lists available at ScienceDirect

Journal of Cleaner Production

journal homepage: www.elsevier.com/locate/jclepro

High-resolution dataset of urban canopy parameters for Beijing and its application to the integrated WRF/Urban modelling system

Xiaodong He [a], Yuhuan Li [a], Xinran Wang [b], Liang Chen [c, d], Bu Yu [e], Yizhou Zhang [a], Shiguang Miao [a, *]

[a] Institute of Urban Meteorology, China Meteorological Administration, 100089 Beijing, China
[b] China Institute of Atomic Energy, 102413 Beijing, China
[c] Key Laboratory of Geographic Information Science (Ministry of Education), East China Normal University, 200241 Shanghai, China
[d] School of Geographic Sciences, East China Normal University, 200241 Shanghai, China
[e] Hangzhou Meteorological Bureau, 310002 Hangzhou, China

ARTICLE INFO

Article history:
Received 31 December 2017
Received in revised form
7 August 2018
Accepted 9 October 2018
Available online 10 October 2018

Keywords:
Beijing
Urban canopy parameters
Urban morphology
WRF/Urban modelling system
Urban environmental issues

ABSTRACT

The Weather Research and Forecasting (WRF) model with urban canopy model has been widely used to study atmospheric boundary layer processes and urbanization-related environmental issues. One of the most daunting challenges faced by the integrated WRF/urban modelling system is constraining the uncertainties in urban canopy parameters (UCPs) that represent the urban morphological characteristics. In this paper, we develop a dataset of three-dimensional (3-D) UCPs for Beijing by using vector-format building information in a Geographic Information System (GIS) environment and apply it to the integrated WRF/urban modelling system to investigate the effects of UCPs on the simulated meteorological variables against observations in clear-sky days. Moreover, the role of spatially-varying UCPs involved in the Building Effect Parameterization (BEP) in capturing the heterogeneous characteristics of 2-m surface air temperature and 10-m wind field in the urban areas are evaluated. In general, high-resolution dataset of UCPs improves the model skill in simulating the diurnal variations and spatial distributions of 2-m surface air temperature and 10-m wind speed in the urban canopy, especially for the BEP. WRF/BEP with gridded UCPs dataset shows a better performance in densely built-up areas, where the morphological and physical characteristics of urban surface are complex. It also performs better in capturing the characteristics of urban heat islands (UHIs) and weak wind zones (WWZs) in urban areas. Results show that introducing the 3-D UCPs dataset into the integrated WRF/urban modelling system is a simple and yet efficient way to enhance the modelling capabilities in urban areas and assist urban planners to deal with urban environmental issues.

1. Introduction

"We shape our dwellings, and afterward our dwellings shape our lives." This intriguing observation came from a speech made by Winston Churchill during the rebuilding of the House of Commons on October 28, 1944. Embedded in the observation is a profound urban climatic and environmental truth regarding the recent rapid global urbanization (He et al., 2015a). With ever-increasing world's urban populations, cities face a series of climatic and environmental issues, such as urban heat islands (UHIs) (Miao et al., 2009; Wang et al., 2016), air pollution (Jiang et al., 2013; Zhang et al., 2015), and extreme weather (Meng and Yao, 2014; Zhang et al., 2014). To improve the performance of regional climate model in simulating urban climate and propose innovative urban adaptation strategies, it becomes necessary to gain a better understanding of the complex interactions of urban surfaces and the atmosphere (Li et al., 2016; Zhang et al., 2009). Various techniques and parameterizations are implemented in regional climate models to represent the urban-induced thermal and dynamic effects. Its main goal is to consider the urban impacts on land surface energy budget and atmospheric boundary layer processes.

The Weather Research and Forecasting (WRF) model is a next-generation mesoscale weather simulation system that can be used effectively for both basic atmospheric research and

* Corresponding author.
E-mail address: sgmiao@ium.cn (S. Miao).

https://doi.org/10.1016/j.jclepro.2018.10.086
0959-6526/

operational weather prediction. WRF is a non-hydrostatic, compressible model with a mass coordinate system in which land surface model (LSM) uses the variables from the atmospheric boundary layer, radiation, cloud microphysics and convective schemes, and the input parameters including the major information about land-surface properties, to calculate surface heat and moisture fluxes (Skamarock et al., 2005). In this paper, we focus the urban modelling efforts on coupling different urban canopy models (UCMs) with Noah LSM in WRF. The single-layer urban canopy model (SLUCM) represents the urban geometry by assuming infinitely-long street canyons, and recognizes the three-dimensional (3-D) nature of urban surfaces (Kusaka et al., 2001; Kusaka and Kimura, 2004). The SLUCM represents the shadowing, trapping and multiple reflections of solar radiation, and prescribes an exponential wind profile in a two-dimensional street canyon. It calculates the surface temperatures of roofs, walls, and roads based on the surface energy budget and estimates the friction velocity and canyon drag coefficient using a similarity stability function for momentum. The calculated surface energy and momentum fluxes are aggregated from urban and non-urban surfaces and passed to the atmospheric boundary-layer scheme in WRF. Anthropogenic heat (AH) and its diurnal variation are taken into consideration by adding them directly to the sensible heat flux from the urban canopy layer (Chen et al., 2011).

The building effect parameterization (BEP) developed by Martilli et al. (2002), represents the most sophisticated urban modelling scheme in WRF. It accounts for the impacts of horizontal (roofs and streets) and vertical (walls) urban surfaces on the prognostic momentum, heat, and turbulent kinetic energy (TKE) fluxes passed to the planetary boundary-layer (PBL). This urban canopy parameterization considers the buildings' drag effects, transformation of mean-motion kinetic energy into TKE, and the modification of surface energy flux due to radiative shadowing and trapping effects. In the BEP, urban grid cells are assumed to be composed of an array of buildings that are located at the same distance and share the same width but different heights. The BEP does not take any type of AH into account (Gutierrez et al., 2015). It should be noted that BEP can well simulate the most frequently observed features of the urban atmosphere, such as the nocturnal UHIs and the elevated inversion layer above the city (Chen et al., 2011).

The internal temperature of the buildings is kept constant in the BEP. A simple building energy model (BEM) has been developed and linked to BEP to improve the estimation of energy exchanges between building interior and the outdoor environment (Salamanca and Martilli, 2010; Chen et al., 2011). The BEM accounts for 1) the diffusion of heat through the walls, roofs, and floors; 2) the radiation passed through windows; 3) the longwave radiation exchanged between indoor surfaces; 4) the generation of heat due to occupants and equipment; and 5) the heat from air conditioning (AC), ventilation, and heating devices. The energy exchanges between building interior and outdoor atmosphere can be well represented by the BEP + BEM parameterization, by which the impacts of AC and its energy consumption can be well estimated consequently (Salamanca et al., 2011).

It is important for the integrated WRF/urban modelling system to capture the effects of complex urban surfaces and morphological features to the development of urban boundary layer (Martilli, 2007; Chen et al., 2011). Recent studies demonstrated that the simulated UHIs, boundary-layer structures, and summer precipitation in the urban areas are sensitive to the parameterization of urban canopy layers, which are in turn heavily affected by the urban morphology determined by a number of urban canopy parameters (UCPs) (Li et al., 2013a, 2016; Salamanca et al., 2011; Miao et al., 2009, 2013b). For the default WRF/urban modelling system, UCPs are traditionally specified in a look-up table as functions of three different urban classes (low-intensity residential, high-intensity residential, and commercial), which may underestimate the heterogeneity and complexities of urban morphology. The National Urban Database and Access Portal Tool (NUDAPT) was developed to provide the requisite gridded dataset of UCPs for urbanized WRF and other advanced urban meteorological, air quality, and climate modelling systems for 44 cities in the United States (Ching et al., 2009). These sets of UCPs account for the aggregated effects of sub-grid building and vegetation morphology on grid-scale properties of the thermodynamics and flow fields within the layer between land surface and the top of the urban canopy. However, such high-resolution dataset of 3-D UCPs is rarely available elsewhere, especially in China.

Beijing is one of the most populated international metropolises in the world with more than 20 million people. Regional climate and environmental condition in megacities with limited land are negatively affected by the concentration of population. The Chinese government has carefully examined these problems and called for scientific urban planning. He et al. (2015b) proposed a numerical-simulation-based method for determining the fresh-air ventilation paths and analysed the seasonal urban weak wind zones (WWZs) and strong wind zones (SWZs) in the urban climate map (UCMap) system of Beijing. For most urban planning applications, a more detailed and high-fidelity flow field is necessarily required. As a consequence, it is urgent to conduct numerical modelling with more realistic UCPs to mitigate and adapt to the evolving environmental issues in the urban areas.

The main objectives of this paper are to 1) introduce the computational methods used for calculating the UCPs in a GIS environment and develop a dataset of 3-D UCPs for Beijing; 2) evaluate the performance of the integrated WRF/urban modelling system with gridded dataset of UCPs in clear-sky days; and 3) evaluate the capacity of WRF/BEP modelling system with gridded UCPs in capturing the spatial distributions of 2-m surface air temperature and 10-m wind speed for densely built-up areas of Beijing.

2. Study area

The city of Beijing is located at the northern tip of the roughly triangular North China Plain (39°26′N-41°04′N, 115°25′E–117°30′E), covering a surface area of 16800 km^2. Beijing city has experienced rapid expansion in recent decade, as seen by the developments of concentric ring roads (RRs). Fig. 1a shows the remote sensing images for urban areas in Beijing. Urban areas in Beijing have increased dramatically since the early 1980s with the completion of the Second RR in 1981. The subsequent additions of the Third RR in 1984, the Fourth RR in 1990, the Fifth RR in 2003, and the Sixth RR in 2008 turned Beijing into a megacity. The Second RR traces the old city walls, and the Sixth RR connects satellite towns in the surrounding suburban areas (He et al., 2015a).

The urban areas between the Second and Fourth RRs are typically highly-developed core regions, covering intense central business districts (e.g., the CBD in the Chaoyang District), Zhongguancun Science and Technology Parks, and high-rise housing, which is the down town (DT) of Beijing. While the old town (OT) within the Second RR covers lower buildings, wide open spaces (e.g., Tiananmen Square), large green parks (e.g., the Temple of Heaven), and watersheds (e.g., Beihai Lake) (Fig. 1b). Regions within the Fourth RR are commonly known as the main urban area, and those beyond the Fourth RR are considered to be the suburbs or outskirts. Satellite images from A to E (Fig. 1c) show the built-up areas of Beijing. Densely built-up areas are mixed with surrounding green spaces, resulting in mixed land-use patterns, which is difficult to be represented and simulated in the grid-based

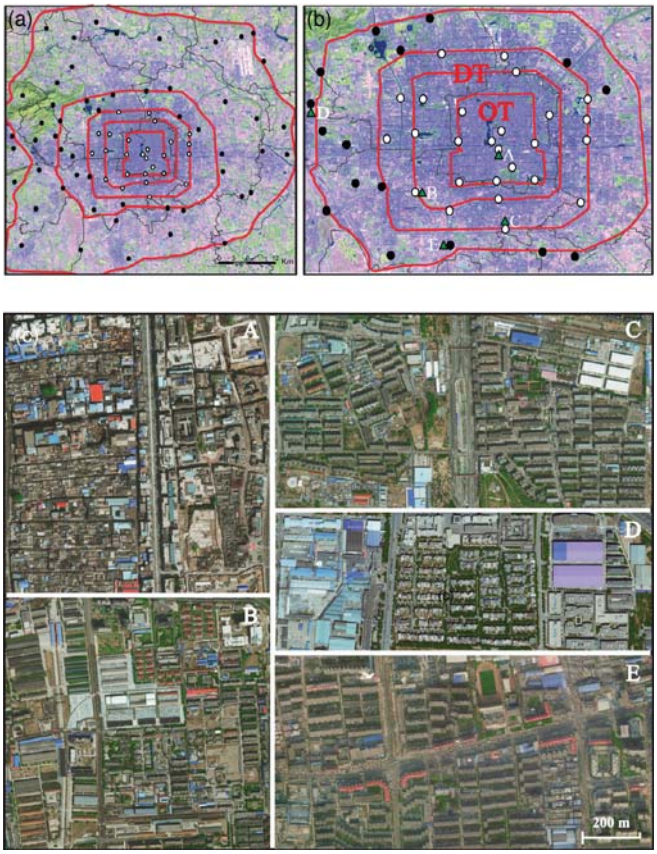

Fig. 1. (a) Remote sensing images of urban areas in Beijing, showing built-up areas (purple), green spaces (green), water bodies (blue), urban AWS sites (white dots) and rural AWS sites (black dots). The red circles represent the Second, Third, Fourth, Fifth and Sixth RRs (from the center outward); (b) Remote sensing images of core urban areas, including DT, OT, and AWS sites near the densely built-up areas (green triangle); (c) Google Earth images of densely built-up areas as marked in Fig. 1b.

modelling system. In addition, the automatic weather stations (AWS) that provide meteorological data (e.g., 2-m surface air temperature, relative humidity, surface pressure, wind speed, etc.) to validate the simulations are concentrated in the urban areas (urban AWS sites, white dots) and their surrounding suburbs (rural AWS sites, black dots) (Fig. 1a).

3. Development of the dataset of urban canopy parameters

3.1. Vector-format building information

The basic geographic information used to calculate the UCPs for Beijing is vector-format building data provided by the Beijing Institute of Surveying and Mapping (Fig. 2). The spatial reference of the updated building data with the geographic Latitude & Longitude projection is GCS_Beijing_1954. The derived shapefile includes a polygon with a series of attributes (e.g., the floors and footprint outline of building, the area and the perimeter of building base, etc.) for each building within the Sixth RR of Beijing.

3.2. Calculation methods

Gridded UCPs used in many atmospheric dispersion models represent the geometrical characteristics of urban morphology that incorporate the effect of spatial distributions of the density, shape, size, and other dominant features of buildings. In this study,

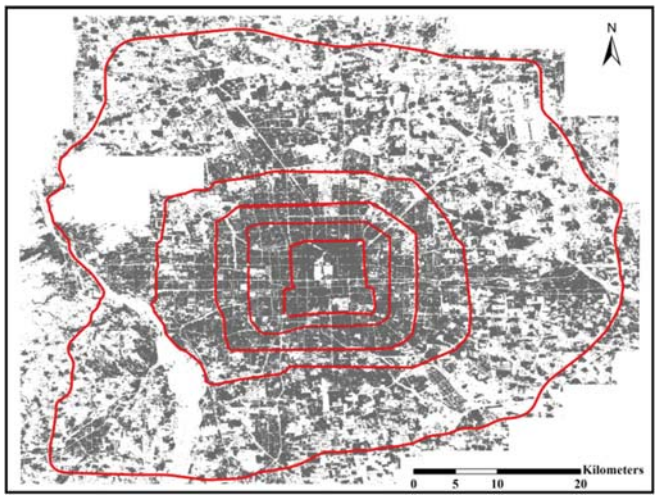

Fig. 2. Vector-format building data within the Sixth RR of Beijing.

ArcGIS-embedded algorithms are developed to create the high-resolution (1 km) dataset of UCPs for Beijing. Corresponding results are saved as raster-format maps in a GIS environment.

3.2.1. Building height characteristics

The mean and standard deviation of building height are calculated as follows:

$$\overline{h} = \frac{\sum_{i=1}^{N} h_i}{N} \tag{1}$$

$$SD = \sqrt{\frac{\sum_{i=1}^{N} \left(h_i - \overline{h}\right)}{N-1}} \tag{2}$$

where $\overline{h}$ is the mean building height, SD is the standard deviation of building height, h_i is the height of building i, and N is the total number of buildings in the area.

The average building height weighted by building plan area is calculated using the following equation:

$$\overline{h}_{AW} = \frac{\sum_{i=1}^{N} A_i h_i}{\sum_{i=1}^{N} A_i} \tag{3}$$

where $\overline{h}_{AW}$ is the mean building height weighted by building plan area, and A_i is the plan area on the ground level of building i.

The histogram of building height is calculated by counting the number of buildings with height falling within specified height interval. Height increment of 5 m is used. The building height histogram with 15 indices is vertically resolved with an increment of 5 m spanning 0–75 m.

3.2.2. Building plan area fraction

The building plan area fraction (λp) is defined as the ratio of the plan area of buildings to the total surface area of the study region:

$$\lambda p = \frac{A_P}{A_T} \tag{4}$$

where A_P is the plan area of buildings at the ground level, i.e., the footprint area, and A_T is the total plan area for the region of interest.

3.2.3. Building surface area to plan area ratio

The building surface area to plan area ratio (λ_B) is defined as the sum of building surface area divided by the total plan area:

$$\lambda_B = \frac{A_R + A_W}{A_T} \tag{5}$$

where A_R is the plan area of rooftops, A_W is the total area of non-horizontal roughness element surfaces (e.g., walls), and A_T is the total plan area for the region of interest.

3.2.4. Frontal area density

The frontal area density (FAD) is a measure of the frontal area per unit horizontal area per unit height increment. It has been widely used in the communities of plant canopy and urban canopy to quantify the drag force as a function of building height. The frontal area density $\lambda_f(z,\theta)$ is defined as follows (Chen and Ng, 2011):

$$\lambda_f(z,\theta) = \frac{A(\theta)_{proj(\Delta z)}}{A_T \Delta z} \tag{6}$$

where $A(\theta)_{proj(\Delta z)}$ is the area of building surfaces projected into the plane that is normal to the approaching wind direction for a specified height increment Δz, θ is the angle of wind direction, and A_T is the total plan area of the study site. The $\lambda_f(z,\theta)$ value for each grid cell in this study is determined for northerly, north-easterly, easterly, and south-easterly winds.

3.2.5. Height-to-width ratio

The height-to-width ratio (λ_S) (also called "street aspect ratio") is calculated for two buildings by dividing the average height by the distance of the two buildings:

$$\lambda_S = \frac{H_1 + H_2}{S_{12}} \tag{7}$$

where H_1 and H_2 are the heights of the upwind and downwind buildings, and S_{12} is the horizontal distance of the two buildings (i.e., the canyon width).

3.2.6. Sky view factor

The sky view factor (SVF) indicates the ratio between the radiations received by a planar surface from the sky to the radiation emitted to the entire hemispheric radiating environment (Watson and Johnson, 1987). It is a dimensionless value ranging from 0 to 1, where SVF = 0 means that the sky is completely obstructed, and the outgoing long-wave radiation is trapped in the urban canyons; SVF = 1 means that the sky is completely open, and the radiation is freely emitted outside the urban canopy layer. Due to its critical role in energy balance schemes, SVF has been commonly used to relate the urban geometry with UHIs in the studies of urban climatology (He et al., 2015a). In general, lower SVF corresponds to stronger UHIs, and vice versa. Chen et al. (2012) proposed an algorithm for the estimate of SVF. Briefly, the method divides the hemispheric radiating environment with radius R into equal slices by a rotation angle α, and searches for a building with the largest elevation angle β along a particular direction. The elevation angle is calculated by the building height. If such a building is found, then the surface S is considered as a slice of an enclosed basin. The view factor of S is calculated as follows (Chen et al., 2012):

$$VF(S) = \left(1 - \cos^2\beta\right) \cdot \left(\frac{\alpha}{360}\right) = \sin^2\beta \cdot \left(\frac{\alpha}{360}\right) \tag{8}$$

After obtaining the $VF(S)$ for all directions, SVF can be calculated by summing up all the $VF(S)$ and subtracting the sum from unity.

3.3. Characteristics of Beijing urban canopy parameters

Fig. 3 presents the percentage of building heights (%) with 5 m bins spanning 0–75 m within the Sixth RR of Beijing. Fig. 4a and b shows the area-weighted average and standard deviation of building heights. DT Beijing is highly developed and has thus gathered high-density and high-rise building groups, while OT Beijing contains lower buildings. As shown in Fig. 4c and d, areas within each RR feature various plan area fraction and building surface area to plan area ratio. Moreover, high-rise but medium-density built-up areas with high building surface ratio can be seen across the northern DT to the Fifth RR due to the newly built residential communities that are mainly concentrated in these

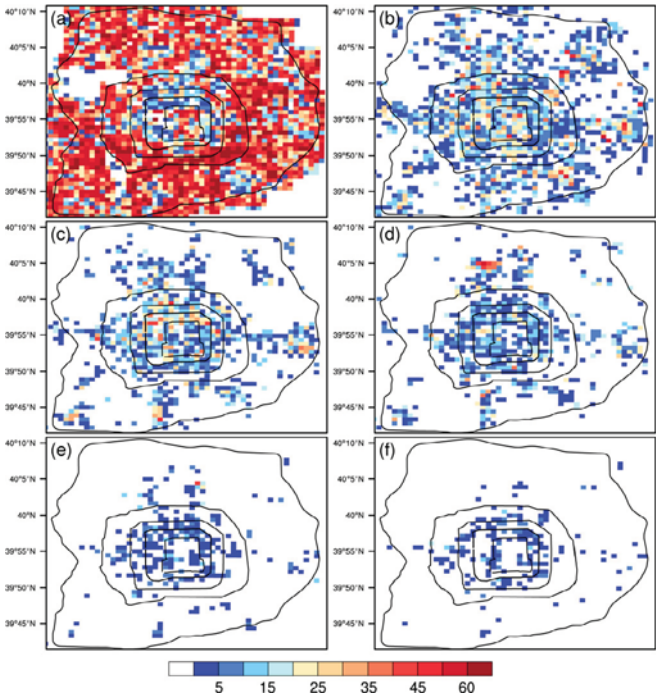

Fig. 3. The percentage of building heights (%) with 5 m bins spanning 0–75 m within the Sixth RR of Beijing: (a) 5 m; (b) 10 m; (c) 15 m; (d) 20 m; (e) 25 m; (f) 30 m.

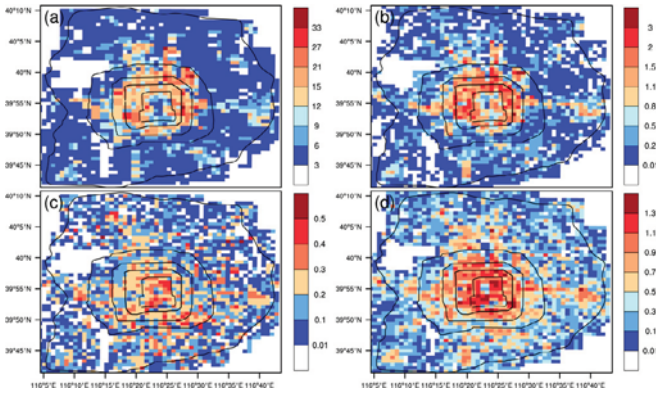

Fig. 4. The spatial distributions of (a) area weighted mean building height (m); (b) standard deviation of building height (m); (c) building plan area fraction (dimensionless); and (d) building surface area to plan area ratio (dimensionless) within the Sixth RR of Beijing.

regions.

The frontal area density considers both the building morphology and the complex wind environment. It has advantages in describing the ventilation conditions and indicating the windward coefficient by building blockage: higher FAD indicates lower ventilation potentials, whereas lower FAD means fewer building bulks and, therefore, higher ventilation potentials. As Fig. 5c shows, the FAD under easterly wind is significantly less than those under other three wind directions, which is closely related to the layout and orientation of buildings, i.e., facing south. Overall, DT Beijing shows lower ventilation potentials in contrast with OT Beijing and the surrounding suburbs. It should be noted that the spatial distributions of SVF and height-to-width ratio are very similar to the area weighted mean building height. Due to space limitations, these figures are not shown in this paper.

4. WRF simulations with different urban canopy models

4.1. WRF configuration

As shown in Table 1, six WRF numerical experiments with three different urban canopy parameterizations were conducted. The only difference between the 'Default' cases and 'New' cases is that the parameters of urban morphology were assigned based on three urban land-use categories (low-intensity residential, high-intensity residential, and commercial) or determined by gridded dataset of UCPs as documented in Table 2. Note that each grid cell has a unique combination of UCPs datasets describing its building, vegetation, and land use features. It is clear that significant distinctions exist between the 3-D UCPs dataset (Section 3) and the default look-up table. Not only the spatial distribution characteristics but also the magnitudes of each parameter represented in the model. Furthermore, the coverages of impervious surface (FRC_URB) for the 'New' cases are different from those in the 'Default' cases (Fig. 6).

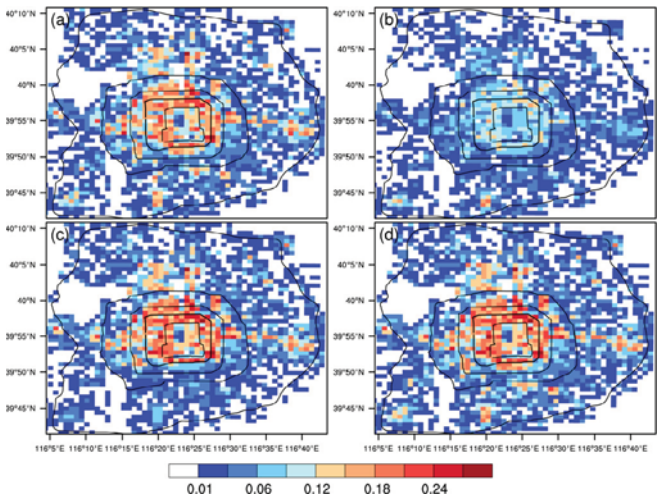

Fig. 5. The spatial distributions of frontal area density (FAD) within the Sixth RR of Beijing: (a) northerly wind; (b) north-easterly wind; (c) easterly wind; and (d) south-easterly wind.

Category-based definition of impervious surface coverages in the 'Default' cases overestimates the extent of commercial district in Beijing largely (Fig. 6a). FRC_URB values in the 'Default' cases are generally larger than those in the 'New' cases, especially for the high-intensity residential and commercial categories (Fig. 6b). In addition, the spatial distributions of FRC_URB in the 'New' cases feature obvious heterogeneity, with relatively lower value (higher permeation) in the center of OT Beijing, whereas the maximum appears around the border of OT Beijing. Fig. 7 shows the distributions of main geometrical urban canyon parameters, which were estimated using the gridded dataset of UCPs following the formulations in Macdonald et al. (1998). These four geometrical urban canyon parameters include zero plane displacement height (Fig. 7a), roughness length above canyon for momentum (Fig. 7b) and heat (Fig. 7c), and roughness length for momentum over roof (Fig. 7d) respectively.

All the simulations have four two-way nested domains (Fig. 8a) centred at (40.24°N, 116.45°E) with horizontal grid spacing (grid numbers) of 27 km (154×154), 9 km (154×154), 3 km (154×154), and 1 km (184×172). The vertical coordinate contains 38 sigma-levels from surface to 50 hPa. We focus the evaluation on the area shown by the rectangle domain 04. Fig. 8 b shows the topographic heights of domain 04.

The physical parameterization schemes used in these simulations include 1) the Dudhia shortwave radiation scheme (Dudhia, 1989); 2) the Rapid Radiative Transfer Model longwave radiation scheme (Mlawer et al., 1997); 3) the TKE scheme Bougeault-Lacarrere (Bougeault and Lacarrere, 1989); 4) the WRF Single-Moment 6-Class Microphysics scheme (Lim and Hong, 2010); 5) the Kain-Fritsc cumulus scheme (Kain, 2004) in domains 01 and 02; and 6) the Noah land-surface model (Chen and Dudhia, 2001) coupled with SLUCM/BEP/BEP + BEM. Simulations were conducted with the initial and boundary conditions provided by the data from the National Center for Environmental Prediction operational Global Final Analyses at a horizontal resolution of 1°×1°.

4.2. Case study

WRF simulations were performed for 7 clear-sky days. For further analysis, we selected one day from 0000 UTC (0800 LST) 5 July 2016 to 0000 UTC (0800 LST) 6 July 2016 to evaluate the performance of the integrated WRF/urban modelling system, when the large-scale synoptic condition was dominated by a uniform high-pressure system over Beijing. Table 3 shows the evaluation results of simulations against observations. The latter are from the AWS stations located in the urban areas of Beijing, including 2-m surface air temperature and 10-m wind speed for the period of 0000 UTC (0800 LST) 5 July 2016 to 0000 UTC (0800 LST) 6 July 2016. All the

Table 1
Overview of the simulation cases with three different urban canopy models.

	Default cases			New cases		
	SLUCM	BEP	BEM	SLUCM_UCPs	BEP_UCPs	BEM_UCPs
How the canopy is resolved	Single layer	Multi-layer	Multi-layer	Single layer	Multi-layer	Multi-layer
How the UCPs are specified	Look-up table	Look-up table	Look-up table	Gridded UCPs dataset	Gridded UCPs dataset	Gridded UCPs dataset
Anthropogenic heat (AH)	From fixed temporal profiles	No	From building energy model	From fixed temporal profiles	No	From building energy model

Table 2
Urban canopy parameters used in the integrated WRF/urban modelling system.

Parameters	Name (Unit)	Default cases (Look-up table)						New cases		
		Low-intensity residential		High-intensity residential		Commercial		(Gridded UCPs dataset)		
ZR	Roof level (mean building height) (m)	8.0		12.0		16.0		MH_URB2D		
SIGMA_ZED	Standard deviation of building height (−)	1.0		3.0		4.0		STDH_URB2D		
BUILD_HEIGHT	Area weighted mean building height (m)	No		No		No		HGT_URB2D		
BUILD_AREA_FRACTION	Building plan area fraction (−)	No		No		No		LP_URB2D		
BUILD_SURF_RATIO	Building surface to plan area fraction (−)	No		No		No		LB_URB2D		
FRC_URB	Fraction of the urban landscape that does not have natural vegetation (−)	0.64		0.83		0.9		FRC_URB2D		
HEIGHT_TO_WIDTH	Height to width ratio (−)	No		No		No		H2W_URB2D		
SVF	Sky view factor (−)	No		No		No		SVF_URB2D		
FRONTAL_AREA_INDEX	Building frontal area index (−)	No		No		No		LF_URB2D		
ROOF_WIDTH[a]	Roof (i.e., building) width (m)	8.3		9.4		10.0		BW_URB2D		
ROAD_WIDTH[a]	Road width (m)	8.3		9.4		10.0		SW_URB2D		
ZDC[a]	Zero plane displacement height (m)	1/5 of ZR		1/5 of ZR		1/5 of ZR		ZDC_URB2D		
Z0C[a]	Roughness length above canyon for momentum (m)	1/10 of ZR		1/10 of ZR		1/10 of ZR		Z0C_URB2D		
Z0HC[a]	Roughness length above canyon for heat (m)	1/10 of Z0C		1/10 of Z0C		1/10 of Z0C		Z0HC_URB2D		
Z0R[a]	Roughness length for momentum over roof (m)	0.01		0.01		0.01		Z0R_URB2D		
Parameters used only in BEP										
Height_bin	Building height bins defined for a particular urban category (m)	5 m bins Spanning 5−15 m		5 m bins Spanning 10−20 m				5 m bins Spanning 15−30 m		5 m bins Spanning 0−75 m
Hpercent_bin	Percentage of a particular urban category populated by buildings of particular height bins (%)	Height (m)	Percentage (%)	Height (m)	Percentage (%)			Height (m)	Percentage (%)	
		5.0	15.0	10.0	20.0			15.0	10.0	HI_URB2D
		10.0	70.0	15.0	60.0			20.0	25.0	
		15.0	15.0	20.0	20.0			25.0	40.0	
								30.0	25.0	

[a] The geometrical urban canyon parameters were estimated using the gridded UCPs dataset following the formulations in Macdonald et al. (1998).

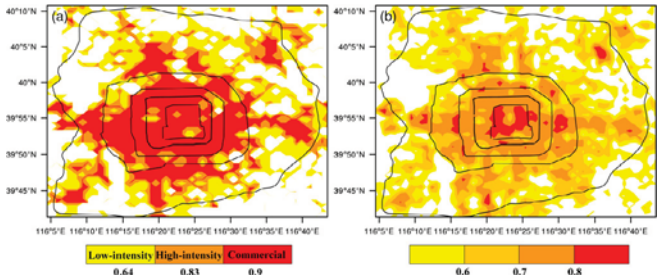

Fig. 6. The spatial distributions of impervious surface coverages (FRC_URB, dimensionless) within the Sixth RR of Beijing: (a) Default cases; (b) New cases.

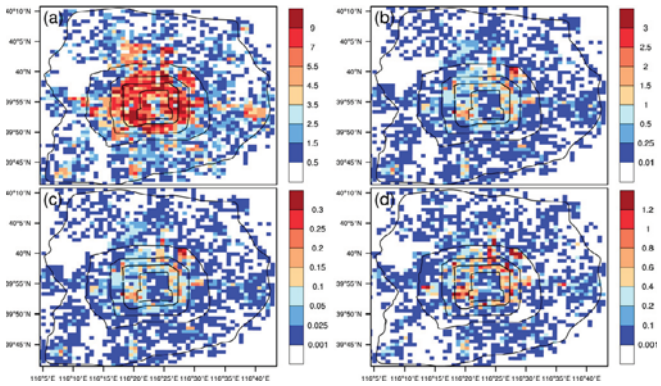

Fig. 7. The spatial distributions of geometrical urban canyon parameters within the Sixth RR of Beijing: (a) zero plane displacement height (m); (b) roughness length above canyon for momentum (m); (c) roughness length above canyon for heat (m); (d) roughness length for momentum over roof (m).

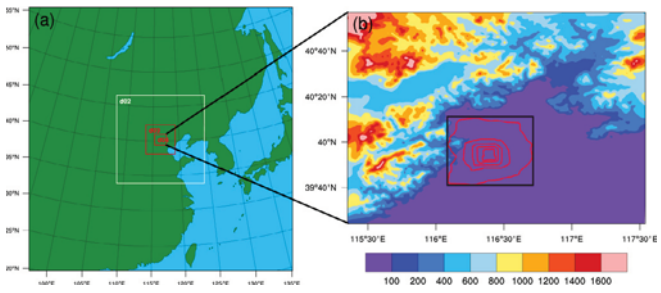

Fig. 8. (a) Configuration of two-way nested domains for WRF simulations; (b) the terrain heights (m) of domain 04. The black rectangle shows the core urban areas in Beijing.

simulations overestimate the 2-m surface air temperature slightly, whereas the 'New' cases yield better results than the 'Default' ones, especially for the BEP parameterization. For BEP_UCPs case, the BIAS and RMSE of 2-m surface air temperature significantly decrease for all the subcategories of urban, and the correlation coefficient between simulation and observations increase markedly. For the WRF/BEP with high-resolution dataset of UCPs or not, there was no significant difference in the simulated 10-m wind speed between the 'Default' and the 'New' case. Meanwhile, the WRF/SLUCM with gridded UCPs dataset performs better with a smaller BIAS and RMSE of 10-m wind speed.

Fig. 9 shows the diurnal variation of simulated and observed 2-m surface air temperature for three urban subcategories. All the simulations tend to overestimate 2-m surface air temperature after 0800 UTC (1600 LST). The 'New' cases generate lower 2-m surface air temperature than the 'Default' ones and agree better with observations, especially for BEP_UCPs. Due to the complexity of the built-up environment, the increase in urban surfaces traps more shortwave radiation and cause more heat storage, particularly at the local noon when the downward shortwave radiation reaches its maximum. At night, urban releases more heat from the ground surface to the overlaying air. Consequently, the diurnal variation of 2-m surface air temperature is better captured in the 'New' cases.

As shown in Fig. 10, little difference in 10-m wind speed can be found between the 'New' and the 'Default' cases. All the cases overestimate the wind speed, especially during the period from sunset at 1200 UTC (2000 LST) to midnight at 1800 UTC (2400 LST). It should be mentioned that WRF/SLUCM with gridded UCPs dataset notably improves the simulation of 10-m wind speed in urban areas. This is associated with that SLUCM_UCPs simulation accounts for the effects of fontal area density from four wind directions, contributing to a better description of the windward coefficient by building blockage in built-up urban areas.

As an example of spatial distributions of surface variables, the simulated 2-m surface air temperature and 10-m wind speed from the BEP and BEP_UCPs cases are shown in Figs. 11 and 12. To better illustrate the maximized effects of urban morphology on surface air temperature and wind speed, we selected the time of 0400 UTC (1200 LST) for comparing the 2-m surface air temperature and 0300 UTC (1100 LST) for comparing the 10-m wind speed. Note that higher 2-m surface air temperature tends to appear between the 2nd and 4th RR, while lower ones expectedly exist inside the 2nd and outside the 4th RR (Fig. 11a). The spatial pattern of surface of air temperature is associated with the spatially-varying characteristics of buildings' height, plan area fractions, and surface area to plan area ratios in DT Beijing. The key finding noted here is that the case of BEP_UCPs (Fig. 11c) performs much better in capturing the spatial heterogeneity for surface air temperature than the 'Default' BEP case (Fig. 11b). The bias in BEP_UCPs case is much smaller than that in the 'Default' BEP case for most stations, particularly in the densely built-up areas (Fig. 1c).

Mean and turbulent wind velocity fields are modified by the buildings' barrier effect, as well as by rougher urban surfaces that increase the frictional drag on the flow (Bornstein and Johnson, 1977). The surface roughness parameter increases from as little as 0.01 cm over mudflats to several meters over built-up urban areas (Oke, 1973). Fig. 12 shows the simulated and observed spatial distribution of 10-m wind speed at 0300 UTC (1100 LST) 5 July 2016. The wind speed between the 2nd and the 4th RR is about 1 m s $^{-1}$ lower than that in other areas (i.e. inside the 2nd RR), which is associated with the urban morphology of Beijing (Fig. 12a). BEP_UCPs case (Fig. 12c) performs better in capturing the spatial distribution of 10-m wind speed and matches the observations more precisely. Fig. 12d and e shows that the bias in BEP_UCPs simulation is smaller than that in the 'Default' BEP case for most urban areas, especially inside the 2nd RR and across the south of urban Beijing.

More importantly, regarding the applications of numerical simulations in urban planning, the mean state of near-surface variables is more required, compared with the pattern for one specific time. Thus, to meet the practical demands for urban planning, the simulated 2-m surface air temperature and 10-m wind speed were averaged during the period from 0000 UTC (0800 LST) 5 July 2016 to 1200 UTC (2000 LST) 5 July 2016, which represents the period for outdoor human activities. Obviously, the BEP_UCPs simulation is more capable for capturing the heterogeneous spatial distribution of 2-m surface air temperature in built-up urban areas (Fig. 13b).

Fig. 14 shows the spatial distribution of the mean 10-m wind speed during the period from 0000 UTC (0800 LST) 5 July 2016 to 1200 UTC (2000 LST) 5 July 2016. BEP_UCPs case performs better in

Table 3
Evaluations of simulated 2-m surface air temperature and 10-m wind speed for the integrated WRF/urban modelling system. Statistic metrics were averaged for the period from 0000 UTC (0800 LST) 5 July 2016 to 0000 UTC (0800 LST) 6 July 2016.

Urban land-use category	Simulation cases	T2 (°C)			W10 (m s^{-1})		
		BIAS (WRF-Obs)	RMSE	R	BIAS (WRF-Obs)	RMSE	R
Commercial	SLUCM	1.89	2.34	0.90	1.70	2.10	0.06
	SLUCM_UCPs	1.42	1.93	0.92	1.20	1.59	0.12
	BEP	0.75	1.09	0.97	0.11	0.40	0.71
	BEP_UCPs	0.19	0.94	0.98	0.23	0.48	0.72
	BEM	2.22	2.56	0.91	0.49	0.69	0.54
	BEM_UCPs	1.61	1.92	0.94	0.57	0.77	0.61
High intensity residential	SLUCM	1.70	2.11	0.92	1.09	1.62	0.18
	SLUCM_UCPs	1.21	1.62	0.94	1.11	1.65	0.20
	BEP	0.77	1.10	0.97	0.04	0.54	0.67
	BEP_UCPs	0.07	0.92	0.98	0.07	0.55	0.67
	BEM	1.87	2.21	0.92	0.32	0.78	0.46
	BEM_UCPs	1.26	1.64	0.94	0.42	0.88	0.47
Low intensity residential	SLUCM	0.93	1.33	0.96	1.52	1.96	0.18
	SLUCM_UCPs	0.49	0.97	0.97	1.59	2.07	0.15
	BEP	0.42	0.73	0.98	0.66	0.87	0.62
	BEP_UCPs	−0.25	0.75	0.98	0.77	0.99	0.57
	BEM	1.07	1.41	0.96	0.95	1.19	0.46
	BEM_UCPs	0.63	1.03	0.97	1.11	1.38	0.41
Urban (the average for three urban categories)	SLUCM	1.63	2.08	0.92	1.60	2.02	0.11
	SLUCM_UCPs	1.16	1.64	0.94	1.28	1.71	0.14
	BEP	0.67	0.99	0.97	0.23	0.47	0.69
	BEP_UCPs	0.07	0.86	0.98	0.34	0.58	0.69
	BEM	1.89	2.23	0.93	0.58	0.80	0.51
	BEM_UCPs	1.32	1.65	0.95	0.68	0.91	0.54

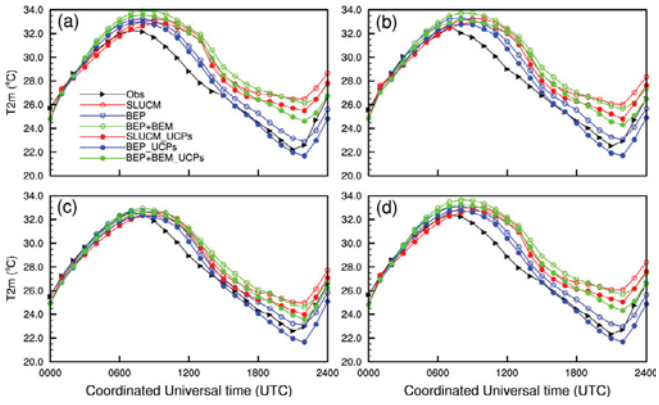

Fig. 9. The diurnal variation of 2-m surface air temperature (°C) in urban stations from 0000 UTC (0800 LST) 5 July 2016 to 0000 UTC (0800 LST) 6 July 2016: (a) commercial, (b) high intensity residential, (c) low intensity residential, (d) urban. Shown are observation (black solid triangle), New cases (solid circle), and Default cases (hollow circle).

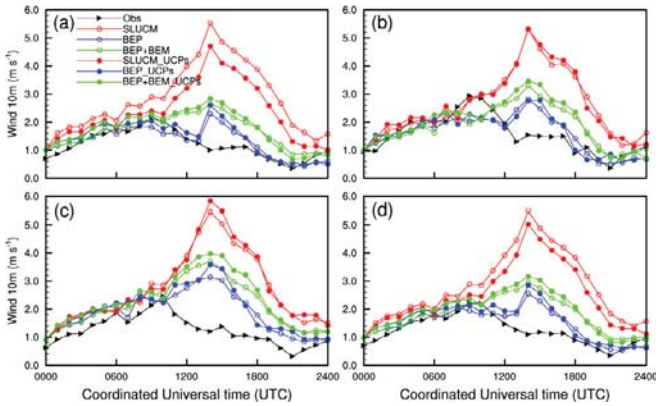

Fig. 10. The diurnal variation of 10-m wind speed (m s^{-1}) in urban stations from 0000 UTC (0800 LST) 5 July 2016 to 0000 UTC (0800 LST) 6 July 2016: (a) commercial, (b) high intensity residential, (c) low intensity residential, (d) urban. Shown are the observation (black solid triangle), New cases (solid circle), and Default cases (hollow circle).

representing the spatial characteristics of wind speeds. Wind flows decelerate when they encounter the high surface roughness at the urban edge (DT Beijing) with the expected larger frontal area density (Fig. 14b). However, with the reduced surface roughness and relatively lower frontal area density in OT Beijing, the wind speed returns to its value in the rural areas. Fig. 14b suggests that WWZs commonly exist within DT Beijing, where the high-rise and high-density buildings are located. By contrast, OT Beijing inversely presents SWZs not only due to the decreased roughness length, but also the UHIs-induced convergence accelerated flows inward the city (Bornstein, 1975). As a comparison, the 'Default' BEP case cannot capture the uneven urban effects on the wind speed (Fig. 14a).

He et al. (2015b) developed the UCMap system of Beijing. The key components of UCMap are the urban climatic analysis map (UC-AnMap) and a set of hierarchical urban climatic classifications within the urban areas in Beijing. The UC– AnMap with a fine resolution of 250 m provides a platform for climatic information and evaluation. It is also named the 'Synthetic Climatic Function Map', summarizing and evaluating the urban thermal load and ventilation potentials. The UC-AnMap within urban Beijing clearly indicates that the hierarchical urban climatic classifications are consistent with the nearly closed 'Single Center + Rings' urban layout of Beijing, which leads to a strong thermal load and poor ventilation in most urban areas within the 4th RR. Note that the BEP_UCPs case effectively reproduced the characteristics of UHIs and WWZs in urban areas, and correctly simulated the strongest UHIs (Fig. 13b) and WWZs (Fig. 14b) in DT Beijing, which is more consistent with the UC-AnMap of urban Beijing. Overall, BEP_UCPs shows a good performance in simulating 2-m surface air temperature and 10-m wind speed for the core urban areas, which is closely related to the underlying surfaces and building morphology.

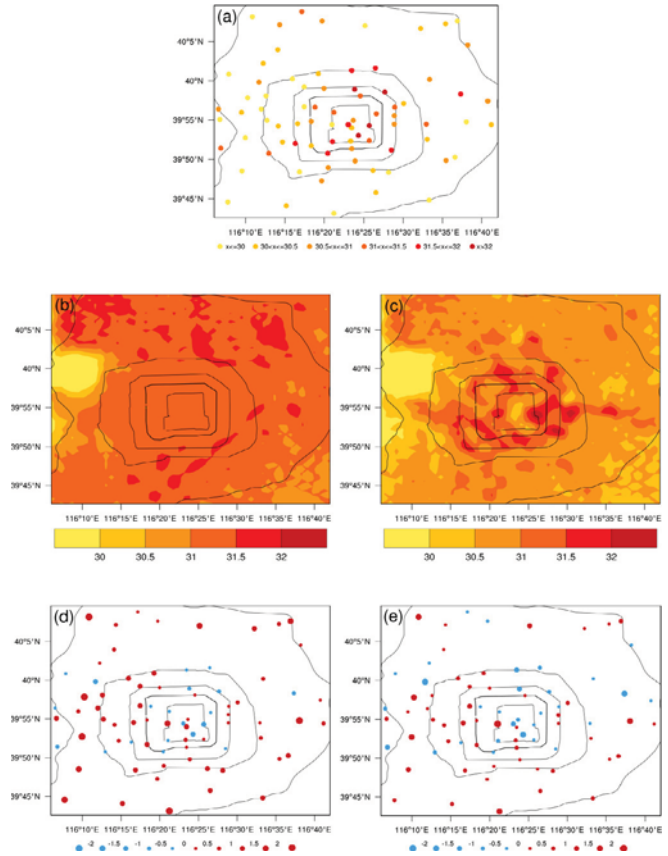

Fig. 11. Spatial distributions of 2-m surface air temperature (°C) at 0400 UTC (1200 LST) 5 July 2016: (a) the observation; (b) BEP; (c) BEP_UCPs; (d) the difference between BEP and observations; (e) the difference between BEP_UCPs and observations.

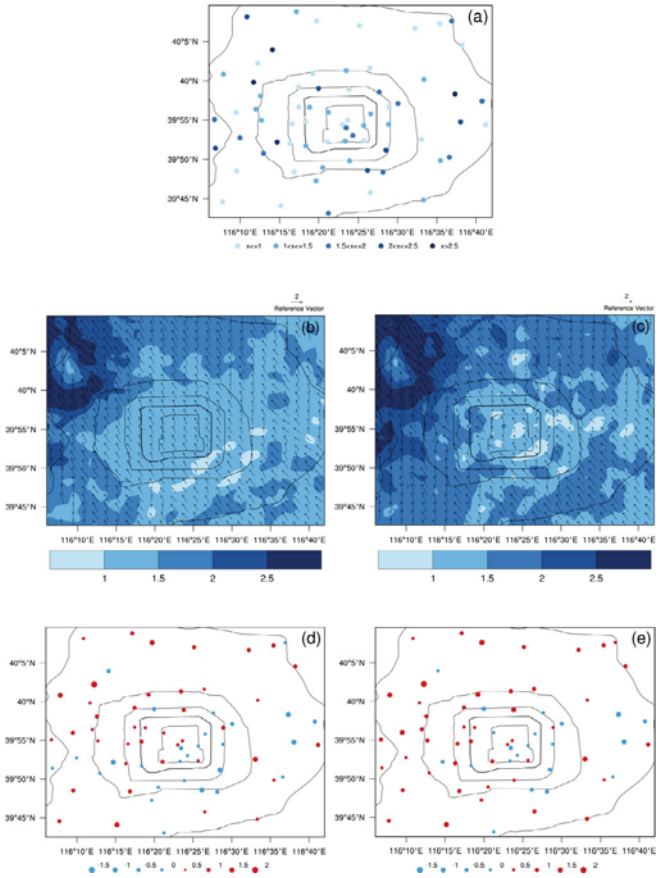

Fig. 12. Spatial distributions of 10-m wind speed (m s^{-1}) at 0300 UTC (1100 LST) 5 July 2016: (a) the observation; (b) BEP; (c) BEP_UCPs; (d) the difference between BEP and observations; (e) the difference between BEP_UCPs and observations.

5. Conclusions and discussions

In this paper, a high-resolution gridded dataset of 3-D UCPs for Beijing was developed by using the vector-format building data in a GIS environment. This unique dataset of UCPs was incorporated into the integrated WRF/urban modelling system to provide more information about vertical characteristics of urban geometry and complex urban surfaces. The effects of updated UCPs on the numerical simulation were evaluated by comparing with observations. Moreover, the capacities of gridded dataset of UCPs involved in WRF/BEP in capturing the heterogeneity of 2-m surface air temperature and 10-m wind field within the city were investigated.

Multi-day simulations with gridded dataset of UCPs were conducted for Beijing, with results compared with the corresponding default WRF/urban canopy models cases. In general, simulations with 3-D UCPs dataset, especially for the BEP_UCPs case, have a more accurate representation of the diurnal and horizontal distributions of 2-m surface air temperature and 10-m wind speed fields in the urban canopy. High-resolution gridded dataset of UCPs acts an important role in simulating the spatial distribution of surface air temperature and wind speed for the integrated WRF/urban modelling system. The 10-m wind speed within DT Beijing in BEP_UCPs case was lower than that in other areas, which is more consistent with observations. BEP_UCPs also reasonably reproduced the spatial characteristics of UHIs and WWZs and correctly simulated the strongest UHIs and WWZs within DT Beijing. WRF/BEP with gridded UCPs dataset involved showed a good performance in the core urban areas, which is related to the underlying surfaces and building morphology.

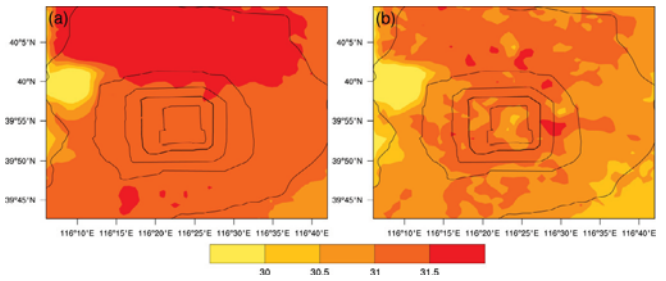

Fig. 13. Spatial distributions of temporal mean 2-m surface air temperature (°C) from 0000 UTC (0800 LST) 5 July 2016 to 1200 UTC (2000 LST) 5 July 2016: (a) BEP; (b) BEP_UCPs.

The specification and development of a comprehensive UCPs dataset, including the sub-grid building morphology, vegetation canopy, traffic emissions, and AH, will still remain a challenge in cities, due to the large disparity in data availability and methodology for mapping fine-scale and highly variable data for the WRF modelling grid (Chen et al., 2011). The accurate and up-to-date information about urban and surrounding environs (e.g., vegetation, water, forest, and cropland) was not available in this study. More efforts are needed to develop the sub-grid vegetation morphology dataset to improve the grid-scale properties of the thermodynamics processes. In addition, more simulations need to be conducted to investigate the effect of the representation of urban surfaces on the simulated precipitation in the integrated WRF/

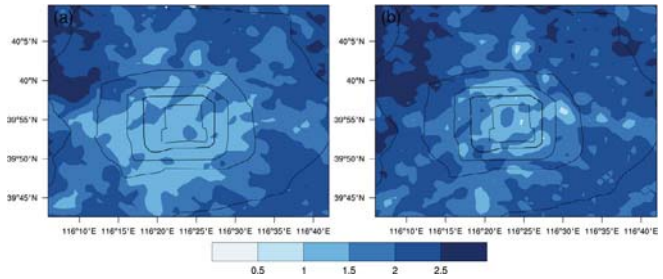

Fig. 14. Spatial distributions of temporal mean 10-m wind speed (m s^{-1}) from 0000 UTC (0800 LST) 5 July 2016 to 1200 UTC (2000 LST) 5 July 2016: (a) BEP; (b) BEP_UCPs.

urban modelling system.

6. Way forward – towards a climate adaptation city

High-rise and high-density cities are becoming an increasing trend due to rapid urbanization in developing countries. Sustainable and climate-friendly spatial planning is one of the most important tasks and challenges for planners and policy-makers given the on-going climate change and public concern for high-quality urban living. Unprecedented challenges include comprehensive understanding of the interrelationship between modern urbanization and local urban climate, and the establishment of a reasonable urban planning system from the perspective of the sustainable development. Therefore, creating the high-resolution dataset of UCPs and studying their effects on local climate is essential for scientific urban planning for a comfortable living environment.

For urban climatologists aiming to assist planners, urban climatic information at the national and regional planning scale with prevailing and critical conditions needs to be confirmed. Moreover, greater spatial detail and fidelity of the thermal environment and flow fields are required. Overall, criticality and the climate-sensitive areas need to be stated so that planners can find ways to prioritize issues. Numerical model serves as an efficient tool to provide additional information and guidance when dealing with urban environmental issues including urban heat islands, weak wind zones, etc.

Acknowledgments

The authors would like to thank Yonghong Liu at the Beijing Municipal Climate Center for processing the data. This work was supported by Beijing Natural Science Foundation (8184071), National Natural Science Foundation of China (41805089 and 41705088), Beijing Municipal Science and Technology Commission (Z161100001116065 and Z151100002115045), and the Ministry of Science and Technology of China (2015DFA20870).

Appendix. A list of abbreviations

Abbreviations and Descriptions

AC	Air conditioning
AH	Anthropogenic heat
AWS	Automatic weather station
BEM	Building energy model
BEP	Building effect parameterization
DT	Down town
FAD	Frontal area density
GIS	Geographic Information System
LSM	Land surface model
NUDAPT	The National Urban Database and Access Portal Tool
OT	Old town
PBL	Planetary boundary-layer
R	Correlation coefficient
RMSE	Root Mean Square Error
RRs	Ring roads
SLUCM	Single-layer urban canopy model
SVF	Sky view factor
SWZs	Strong wind zones
TKE	Turbulent kinetic energy
UC-AnMap	Urban climatic analysis map
UCMap	Urban climate map
UCMs	Urban canopy models
UCPs	Urban canopy parameters
UHIs	Urban heat islands
WRF	Weather Research and Forecasting model
WWZs	Weak wind zones
3-D	Three-dimensional

References

Bornstein, R.D., 1975. The two-dimensional URBMET urban boundary layer model. J. Appl. Meteorol. Climatol. 14, 1459–1477.
Bornstein, R.D., Johnson, D.S., 1977. Urban-rural wind velocity differences. Atmos. Environ. 11, 597–604.
Bougeault, P., Lacarrere, P., 1989. Parameterization of orography-induced turbulence in a mesobeta-scale model. Mon. Weather Rev. 117, 1872–1890.
Chen, F., Dudhia, J., 2001. Coupling an advanced land surface–hydrology model with the Penn State–NCAR MM5 modeling system. Part I: model implementation and sensitivity. Mon. Weather Rev. 129 (4), 569–585.
Chen, F., Kusaka, H., Bornstein, R., Ching, J., Grimmond, C.S.B., et al., 2011. The integrated WRF/urban modelling system: development, evaluation, and applications to urban environmental problems. Int. J. Climatol. 31 (2), 273–288.
Chen, L., Ng, E., 2011. Quantitative urban climate mapping based on a geographical database: a simulation approach using Hong Kong as a case study. Int. J. Appl. Earth. Obs 13, 586–594.
Chen, L., Ng, E., An, X.P., Ren, C., Lee, M., et al., 2012. Sky view factor analysis of street canyons and its implications for daytime intra-urban air temperature differentials in high-rise, high-density urban areas of Hong Kong: a GIS-based simulation approach. Int. J. Climatol. 32, 121–136.
Ching, J., Brown, M., McPherson, T., et al., 2009. National urban database and access portal tool, NUDAPT. Bull. Am. Meteorol. Soc. 90, 1157–1168.
Dudhia, J., 1989. Numerical study of convection observed during the winter monsoon experiment using a mesoscale two-dimension model. J. Atmos. Sci. 46 (20), 3077–3107.
Gutierrez, E., Gonzalez, Martilli, A., Bornstein, R., Arend, M., 2015. Simulations of a heat-wave event in New York city using a multilayer urban parameterization. J. Appl. Meteorol. Climatol. 54, 283–300.
He, X.D., Miao, S.G., Shen, S.H., Li, J., Zhang, B.Z., et al., 2015a. Influence of sky view factor on outdoor thermal environment and physiological equivalent temperature. Int. J. Biometeorol. 59 (3), 285–297.
He, X.D., Shen, S.H., Miao, S.G., Dou, J.J., Zhang, Y.Z., 2015b. Quantitative detection of urban climate resources and the establishment of an urban climate map (UCMap) system in Beijing. Build. Environ. 92, 668–678.
Jiang, P., Chen, Y., Geng, Y., Dong, W., Xue, B., et al., 2013. Analysis of the co-benefits of climate change mitigation and air pollution reduction in China. J. Clean. Prod. 58, 130–137.
Kain, J.S., 2004. The Kain-Fritsch convective parameterization: an update. J. Appl. Meteorol. 43 (1), 170–181.
Kusaka, H., Kondo, H., Kikegawa, Y., Kimura, F., 2001. A simple single layer urban canopy model for atmospheric models: comparison with multi-layer and slab models. Bound-Lay Meteorol. 101, 329–358.
Kusaka, H., Kimura, F., 2004. Coupling a single-layer urban canopy model with a simple atmospheric model: impact on urban heat island simulation for an idealized case. J. Meteorol. Soc. Jpn. 82, 67–80.
Li, D., Bou-Zeid, E., Baeck, M.L., Jessup, S., Smith, J.A., 2013a. Modeling land surface processes and heavy rainfall in urban environments: sensitivity to urban surface representations. J. Hydrometeorol. 14 (8), 1098–1118.
Li, D., Bou-Zeid, E., Barlage, M., Chen, F., Smith, J.A., 2013b. Development and evaluation of a mosaic approach in the WRF-Noah framework. J. Geophys. Res. Atmos. 118, 11918–11935.
Li, Y.H., Miao, S.G., Chen, F., Liu, Y.H., 2016. Introducing and evaluating a new building-height categorization based on the fractal dimension into the coupled WRF/urban model. Int. J. Climatol. 37 (7), 3111–3122.
Lim, K.S.S., Hong, S.Y., 2010. Development of an effective double-moment cloud microphysics scheme with prognostic cloud condensation nuclei (CCN) for weather and climate models. Mon. Weather Rev. 138 (138), 1587–1612.

Macdonald, R.W., Griffiths, R.F., Hall, D.J., 1998. An improved method for the estimation of surface roughness of obstacles arrays. Atmos. Environ. 32 (11), 1857–1864.
Martilli, A., Clappier, A., Rotach, M.W., 2002. An urban surface exchange parameterization for mesoscale models. Bound.-Lay. Meteorol. 104, 261–304.
Martilli, A., 2007. Current research and future challenges in urban mesoscale modeling. Int. J. Climatol. 27, 1909–1918.
Meng, Z., Yao, D., 2014. Damage survey, radar, and environment analyses on the first-ever documented tornado in Beijing during the heavy rainfall event of 21 July 2012. Weather Forecast. 29 (6), 702–724.
Miao, S.G., Chen, F., Lemone, M.A., Tewari, M., Li, Q.C., et al., 2009. An observation and modeling study of characteristics of urban heat island and boundary layer structures in Beijing. J. Appl. Meteorol. Climatol. 48 (3), 484–501.
Mlawer, E.J., Taubman, S.J., Brown, P.D., Iacono, M.J., Clough, S.A., 1997. Radiative transfer for inhomogeneous atmospheres: RRTM, a validated correlated-k model for the longwave. J. Geophys. Res. Atmos. 102 (D14), 16663–16682.
Oke, T.R., 1973. Review of Urban Climatology 1968-1973. W.M.O. Report No. 383, TN No. 134, p. 132.
Salamanca, F., Martilli, A., 2010. A new building energy model coupled with an urban canopy parameterization for urban climate simulations-Part II. Validation with one dimension off-line simulations. Theor. Appl. Climatol. 99, 345–356.
Salamanca, F., Martilli, A., Tewari, M., Chen, F., 2011. A study of the urban boundary layer using different urban parameterizations and high-resolution urban canopy parameters with WRF. J. Appl. Meteorol. Climatol. 50, 1107–1128.
Skamarock, W.C., Klemp, J.B., Dudhia, J., Gill, D.O., Barker, D.M., et al., 2005. A Description of the Advanced Research WRF Version 2. NCAR Technical Note TN-468+STR, 88 [Available from NCAR, P. O. Box 3000, Boulder, CO 80307].
Wang, C.D., Wang, Y.T., Geng, Y., Wang, R.Q., Zhang, J.Y., 2016. Measuring regional sustainability with an integrated social-economic-natural approach: a case study of the Yellow River Delta region of China. J. Clean. Prod. 114, 189–198.
Watson, I.D., Johnson, G.T., 1987. Graphical estimation of sky view-factors in urban environments. Int. J. Climatol. 7, 193–197.
Zhang, C.L., Chen, F., Miao, S.G., Li, Q.C., Xia, X.X., et al., 2009. Impact of urban expansion and future green planting on summer precipitation in the Beijing metropolitan area. J. Geophys. Res. 114 (D02116) https://doi.org/10.1029/2008JD010328.
Zhang, H., Wang, S., Hao, J., Wang, X., Wang, S., et al., 2015. Air pollution and control action in Beijing. J. Clean. Prod. 1519–1527.
Zhang, Y., Smith, J.A., Luo, L., Wang, Z., Beack, M.L., 2014. Urbanization and rainfall variability in the Beijing metropolitan region. J. Hydrometeorol. 15 (12), 2219–2235.